ELSEVIER

Chemical Geology 174 (2001) 307–319

CHEMICAL GEOLOGY
INCLUDING
ISOTOPE GEOSCIENCE

www.elsevier.com/locate/chemgeo

High-resolution XANES spectra of iron in minerals and glasses: structural information from the pre-edge region

L. Galoisy *, G. Calas, M.A. Arrio

Laboratoire de Minéralogie-Cristallographie, UMR CNRS 7590, Universités Paris 6 et 7 et IPGP, 4 Place Jussieu, F-75252 Paris Cedex 05, France

Accepted 9 February 2000

Abstract

High-resolution X-ray Absorption Near-Edge Structure (XANES) spectra of iron allow to take into account the effects of the coordination numbers on the quantification of redox values. Volcanic glasses show split pre-edge features, arising from a bimodal distribution between the relative contributions of ferric and ferrous iron. The chemical shift between these two oxidation states, 2 eV, has been resolved using a 400 Si monochromator. High-resolution pre-edge spectroscopy shows the distribution of ferric and ferrous iron between various coordination states. Ferrous iron is mostly fivefold-coordinated and minority fourfold-coordinated while ferric iron occurs in fourfold and sixfold-coordinated sites. The importance of $^{6}Fe^{3+}$ in basaltic glasses may explain the formation of magnetite during glass oxidation. The increase of $^{4}Fe^{3+}$ in the more silicic, pantelleritic glass is consistent with the peralkaline character of this glass. The increase of the proportion of tetrahedral Fe^{3+}, accompanied by more covalent Fe^{3+}–O bonds, is consistent with the chemical dependence of redox equilibria in magmatic systems, in which the most differentiated terms correspond to more oxidizing compositions.

Keywords: Volcanic glass; X-ray spectroscopy; Redox; Coordination; Iron

1. Introduction

The knowledge of the relationships between the structure of glasses or melts and their thermodynamical, physical and chemical properties helps understand the formation conditions of magmas, including redox evolution and mineral formation from melts. Iron has long been known to play an important role in magmatic liquids. The presence of different iron oxidation states with distinct structural roles influences melt properties (Waychunas et al., 1988; Cooney and Sharma, 1990; Jackson et al., 1993) and especially density (Dingwell and Brealey, 1988; Dingwell et al., 1988), viscosity (Dingwell, 1989; Dingwell and Virgo, 1987, 1988) and heat capacity (DeYoreo et al., 1990). The determination of the sites occupied by iron-oxidation states in glasses may then shed light on the evolution mechanisms of silicate magmas.

The surrounding of ferrous and ferric iron in silicate melts and glasses has often been discussed in terms of four or/and six coordinations. However, the presence of fourfold and fivefold-coordinated

* Corresponding author. Fax: +33-1-4427-3785.
E-mail address: galoisy@lmcp.jussieu.fr (L. Galoisy).

0009-2541/01/$ - see front matter
PII: S0009-2541(00)00322-3

species seem to correspond to most recent observations (see, e.g., Galoisy and Calas, 1993; Brown et al., 1995). In addition, few data exist on iron structural surrounding in natural glasses, such as tektites and terrestrial or planetary volcanic glasses. The iron oxidation state is mostly determined using Mössbauer spectroscopy (Regnard et al., 1981; Helgason et al., 1992; Kostov and Yanev, 1996) and wet chemical analyses (Barberi et al., 1973; Auric et al., 1982). Some spectroscopic data are available on these natural glasses, including crystal field spectroscopy on lunar basaltic glasses (Nolet et al., 1979; Dyar and Burns, 1981) or Extended X-ray Absorption Fine Structure (EXAFS) of basaltic glasses and obsidians (Henderson et al., 1995). These data have been interpreted by the presence of octahedral ferrous iron and tetrahedral ferric iron. More recently, an analysis of Mössbauer spectra of tektites, taking into account site distribution effects, has shown that ferrous iron is mainly fivefold-coordinated with some minor fourfold-coordinated sites (Rossano et al., 1999a,b). We present in this paper new data given by high-resolution X-ray Absorption Near-Edge Structure (XANES) spectroscopy, a method sensitive, at the same time, to valence and site geometry concerning a specific element.

XANES spectra show important variations among minerals and glasses as a result of structural and chemical modifications of the investigated element and its surrounding (Waychunas et al., 1983; Brown et al., 1988). Pre-edge features are always observed on the low-energy side of K-absorption edges of first-row transition elements. These features arise from 1s∅3d bound state electronic transitions and are well separated from the slope of the main edge. Although these electric dipole transitions are forbidden in a centrosymmetric environment, weak features are actually observed due to quadrupole coupling effects (Shulman et al., 1976; Dräger et al., 1988; Westre et al., 1997). In a noncentrosymmetric environment, a marked increase in intensity occurs as a result of the metal 3d–4p orbital mixing and metal 3d-ligand 2p-orbital overlap, which relax the forbidden character of the electric dipole transition. Site distortion increases pre-edge intensity (Wong et al., 1984). The dependence of the position of the pre-edge feature on Fe oxidation state has been recently used to determine the Fe redox ratio in minerals (Bajt et al., 1994; Delaney et al., 1996, 1998).

In this paper, high-resolution Fe–K edge XANES spectra of crystalline references have been used to determine iron oxidation states and site geometry in volcanic glasses. Under high instrumental resolution, Fe–K edge XANES spectra often show split pre-edge features in minerals and glasses (Fig. 1). If only one oxidation state is present, this may correspond to spectrally resolved electronic transitions from core levels to the first empty states, as in the Fe–K edge XANES spectrum of andradite garnet (Fig. 1a) .

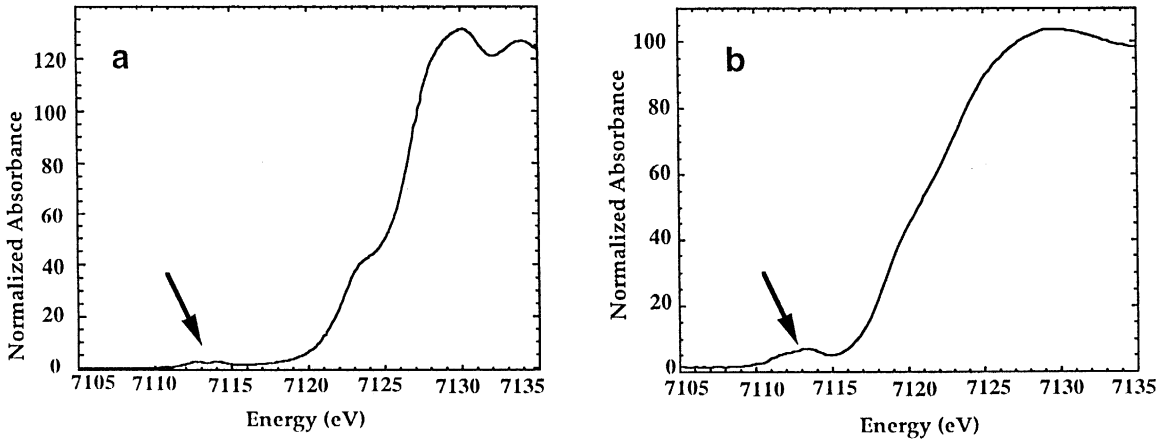

Fig. 1. Fe K-edge XANES spectra of andradite (reference for $^{6}Fe^{3+}$) (a) and oxidized basalt glass (b), showing the split pre-edge on the low energy side of the main edge (arrows).

When iron occurs in the ferrous and ferric oxidation states, as in volcanic glasses, the pre-edge is also split (Fig. 1b), though the pre-edge features are not at the same energy as when only one oxidation state is present. It is then necessary to decipher the respective contribution of both oxidation states. The pre-edge position shows a bimodal distribution within the experimental uncertainty (0.2 eV), between the respective contribution of ferrous and ferric iron. On another hand, the Fe coordination geometry affects both the shape and intensity of the pre-edge. The pre-edge region may then be used to get quantitative information on the oxidation state and local environment around Fe^{2+} and Fe^{3+} in volcanic glasses. Ferric iron occurs in fourfold and sixfold coordination in the three volcanic glasses investigated, and the ratio between $^{4}Fe^{3+}$ and $^{6}Fe^{3+}$ is higher in basaltic than in pantelleritic glasses. This arises from the presence of alkali cations, which are able to charge compensate tetrahedral Fe^{3+}. The pre-edge contribution due to Fe^{2+} is consistent with the presence of low-coordinated ferrous iron, as shown recently in tektites (Rossano et al., 1999a,b). The influence of glass composition on iron coordination may explain the chemical dependence of redox equilibria in silicate melts/glasses.

2. Experimental

2.1. Samples

The minerals used as crystalline references include siderite ($FeCO_3$) and staurolite ($Fe_4Al_{18}Si_8O_{46}(OH)_2$) (Brittany, France) for $^{6}Fe^{2+}$ and $^{4}Fe^{2+}$, respectively, and andradite ($Ca_3Fe_2Si_3O_{12}$; Val Malenco, Italy) for $^{6}Fe^{3+}$. The spectrum of synthetic Fe-berlinite ($FePO_4$) is used as reference for $^{4}Fe^{3+}$ (Combes et al., 1989). Synthetic YIG garnet ($Y_2Fe_5O_{12}$) was used to test the influence of site distribution on pre-edge spectroscopy, as 60% and 40% of Fe^{3+} are fourfold- and sixfold-coordinated, respectively. Other mineral references include synthetic fayalite (Fe_2SiO_4) and hypersthene ($Fe_{0.2}Mg_{1.8}Si_2O_6$: Bamble, Norway), for $^{6}Fe^{2+}$, synthetic $FeAl_2O_4$ spinel for $^{4}Fe^{2+}$ and Garfield nontronite and acmite ($NaFeSi_2O_6$, Mont Saint Hilaire, Quebec) for $^{6}Fe^{3+}$. A Fe^{2+}-bearing glass of composition $0.4MgO–0.4CaO–0.2FeO–SiO_2$, referred hereafter as an augite glass, was synthesized at 1400°C under a $H_2–CO_2$ atmosphere, close to the Fe–FeO buffer. The absence of ferric iron was checked by EPR. A $Na_2Si_2O_5$ glass containing 3 wt.% Fe was synthesized in air at 1100°C, with 80% Fe^{3+} and 20% Fe^{2+}.

Three volcanic glasses (Table 1) were chosen according to their redox ratio:

- Pele's hairs from Erta'Ale, a pure glassy alkaline basalt (Barberi et al., 1973);
- an oxidized, crystal free glass of tholeiitic composition from the Holyoke Basalt Flow (Westfield, USA), which has been melted twice at 1500°C for 16 h in air, quenched and annealed at 525°C;
- a glassy pantellerite (Boïna, Ethiopia) that contains minor crystals of anorthoclase, the triclinic member of the high albite–high sanidine series of alkali feldspars (Barberi et al., 1974).

2.2. Pre-edge spectra acquisition and data analysis

Room-temperature iron–K edge XANES spectra were recorded at the LURE-DCI synchrotron radiation facility (Orsay, France). Ring conditions were 1.54 GeV positron energy and 200-mA positron

Table 1
Chemical composition (wt.%) of the studied volcanic glasses

	Erta'Ale[a]	Boina[b]	Oxidized basalt[c]
SiO_2	49.83	68.43	52.00
Al_2O_3	13.92	11.10	14.10
Fe_2O_3	2.01	3.51	6.78
FeO	9.31	3.59	6.02
MnO	0.19	0.19	
MgO	6.38	< 0.01	6.40
CaO	11.33	0.56	9.30
Na_2O	2.88	6.00	3.20
K_2O	0.64	4.50	1.20
TiO_2	2.36	0.26	1.00
P_2O_5	0.34	0.04	
H_2O^+	0.39	0.76	
H_2O^-	0.09	0.15	
Total	99.69	99.10	100.00
$Fe^{3+}/\Sigma Fe$, %	18	49	53

[a] Barberi et al., 1973.
[b] Barberi et al., 1974.
[c] Bandopadhyay et al., 1980.

current. X-ray energy was monochromatized using a Si(400) channel cut crystal. Due to the large Bragg angle (40°), the experimental resolution is as low as 1 eV in the beam geometry used, which gives an overall energy resolution of about 1.5 eV at the Fe–K edge, including core-hole effects. Pre-edge spectra were recorded using 0.1 eV steps. Energy was calibrated using a metallic Fe foil and checked before and after each scan and did not vary more than 0.2 eV within the experimental session. The absolute energy scale was defined relative to the absorption maximum of the XANES main edge of metallic Fe at 7130.5 eV (Scott et al., 1982).

The fitting procedure is a modification of a method previously described (Calas and Petiau, 1983a). The XANES spectra are normalized to the atomic absorption. The pre-edge is then extracted by subtracting an arctangent function fitting the tail of the main edge from the observed spectra. Pre-edge intensity is normalized to the atomic absorption extrapolated at the same energy and expressed in percent units. The pre-edge of the crystalline references is adjusted with a minimum number of pseudo-Voigt functions accounting for the number of electronic transitions expected from Crystal Field Theory. This analytical procedure agrees with calculations based on a Ligand Field Multiplet Model on the same reference compounds (Arrio et al., submitted). The width of these pseudo-Voigt components has been fixed at 1.5 eV. This value arises from the convolution of the natural width of the 1s∅3d electronic transition by the instrumental resolution. This latter is minimized using high-order (*hkl*) planes, such as the Si(400) reflection used in this study. Because of the importance of site distribution effects, which will affect the position and intensity of the pseudo-Voigt components, a detailed fit of pre-edge spectra of synthetic glasses has not been undertaken.

By contrast to ferrous iron, which suffers important site distribution (Rossano et al., 1999a,b), Fe^{3+} occurs in well-characterized sites (Mysen, 1988). To model both the site occupancy and the oxidation states of iron in volcanic glasses, we have then used a linear combination of the augite glass spectrum, representative of the Fe^{2+} contribution in a silicate glass, together with the sum of pseudo-Voigt components representing the contribution of $^{6}Fe^{3+}$ and $^{4}Fe^{3+}$ extracted from andradite and Fe-berlinite, respectively. This leaves the possibility to account for possible coordination changes of ferric iron as a function of glass composition. These components were adjusted to the experimental spectrum with a least square fitting procedure using the minimization of a χ^2 test. Different criteria were defined to ensure the reliability of the fit: (i) the sum of the various components of the fit must be as close as possible to unity, and any deviation will indicate a modification of the site surrounding as compared to the chosen references; (ii) a good adjustment of the pre-edge will confirm the adequacy of these references; and (iii) the redox state of iron in the glass, defined by the relative contributions of the Fe^{2+} and Fe^{3+} components, should be close to that determined using chemical analyses. Such an analysis shows that a good redox determination should take into account the actual geometry of the sites occupied by ferrous and ferric iron in the glass, and that a previous knowledge of this redox state will, in turn, give more accurate information on the sites occupied by these cations.

3. Results and discussion

3.1. Fe pre-edge spectroscopy in reference minerals

The general shape of the Fe^{2+} and Fe^{3+} XANES spectra in minerals and glasses has been already described (Calas and Petiau, 1983a; Brown et al., 1995; Manceau and Gates, 1997). With high-resolution monochromators, such as Si(400) at the Fe–K edge, a split pre-edge appears on the low-energy side of the main edge (Fig. 1). Crystal field effects cause the splitting of the 3d orbitals. A $(Z+1)$ model accounts for the core hole effects caused by the photon absorption process (Shulman et al., 1976; Calas and Petiau, 1983a; Manceau et al., 1990) and we have considered the 3d-electronic level diagrams of Co^{2+} and Co^{3+} to account for the absorption features observed in the pre-edge of Fe^{2+} and Fe^{3+}, respectively.

3.1.1. Fe^{2+} in octahedral and tetrahedral coordination

In octahedral symmetry, the $1s \rightarrow 3d$ transitions are formally electric dipole forbidden and may gain

intensity from their quadrupolar character. The ($Z+1$) model predicts ^{4}F and ^{4}P free ion states. Three electronic levels give rise to transitions from the 1s core level (Fig. 2a), as the transition to the $^4A_{2g}(^4F)$ level corresponds to a two-electron transition, which has a low probability. By contrast, in tetrahedral symmetry (Td), the dipolar character of the transitions increases due to the absence of an inversion center, giving rise to a significant hybridization of the 3d and 4p levels. Four electronic transitions are, thus, expected (Fig. 2b).

Siderite contains Fe^{2+} cations located in a slightly distorted octahedron with a quadratic elongation (Q.E.) of 1.0013 (Robinson et al., 1971). The pre-edge shows a main peak at 7095.7 eV with a distinct shoulder located at 7097.9 eV. The intensity of the shoulder is half that of the main peak. A small shoulder is visible on the right side of the main peak at 7112.7 eV, which allows to use three pseudo-Voigt components (50% of a Gaussian function and 50% of a Lorentzian function) to fit the pre-edge spectrum. The presence of these three pseudo-Voigt components (Fig. 3a) is in accordance with the number of expected transitions (Westre et al., 1997). The position, relative intensity and transition assignment of the bands are given in Table 2. The intensity of the pre-edge at its maximum is 2.2, which is similar to the values reported for coordination compounds with Fe^{2+} in an OH symmetry (Westre et al., 1997). The influence of stronger site distortions may be studied on the pre-edges of fayalite (Q.E. = 1.0379) and hypersthene (Q.E. > 1.05) (Fig. 3a). In these minerals, the apparent position of the two peaks composing the pre-edge changes: the main peak and the shoulder are shifted by +0.3 eV and −0.2 eV, respectively, as compared to the pre-edge spectrum of siderite. As a consequence, the pre-edge appears to be narrower and less resolved than in siderite. The intensity of the major peak increases by 1.25 and 2 in fayalite and hypersthene, respectively, relative to siderite. The intensity of the shoulder is enhanced to 80% of the main peak intensity for both silicates. This marked changes of the shape of the pre-edges of fayalite and hypersthene as compared to the pre-edge of siderite seems to be the result of the Fe^{2+} 4p–3d orbitals hybridization related to the various types of distortion of the octahedral sites occupied by iron (Galoisy et al., 1999).

In staurolite, Fe^{2+} is located in a slightly distorted tetrahedral site (Q.E. = 1.0004). The pre-edge spectrum is made of a major peak at 7112 eV and a shoulder at 7114 eV, with an intensity half that of the major peak, as for octahedral Fe^{2+}. The intensity of the pre-edge is dramatically enhanced, and five times higher than for Fe^{2+} in an octahedral site (10.8 vs. 2.2), due to the more efficient hybridization of 3d and 4p levels. Similar intensities have been reported for tetrahedral Fe^{2+} in iron coordination compounds (Westre et al., 1997). Four pseudo-Voigt components have been used to simulate the 1s → 3d transitions

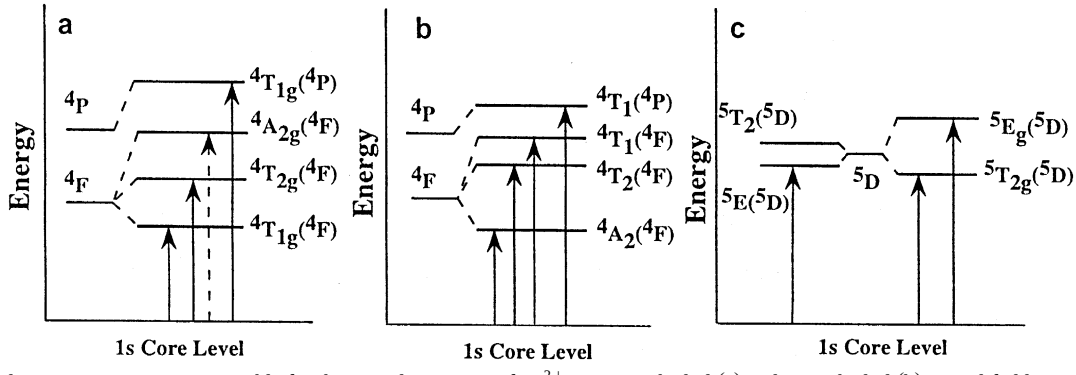

Fig. 2. Electronic transitions responsible for the pre-edge spectra of Fe^{2+} in an octahedral (a) and a tetrahedral (b) crystal field, in a ($Z+1$) model (see text). In (c), the electronic transitions responsible for the pre-edge spectrum of octahedral Fe^{3+} (right) and tetrahedral Fe^{3+} (left).

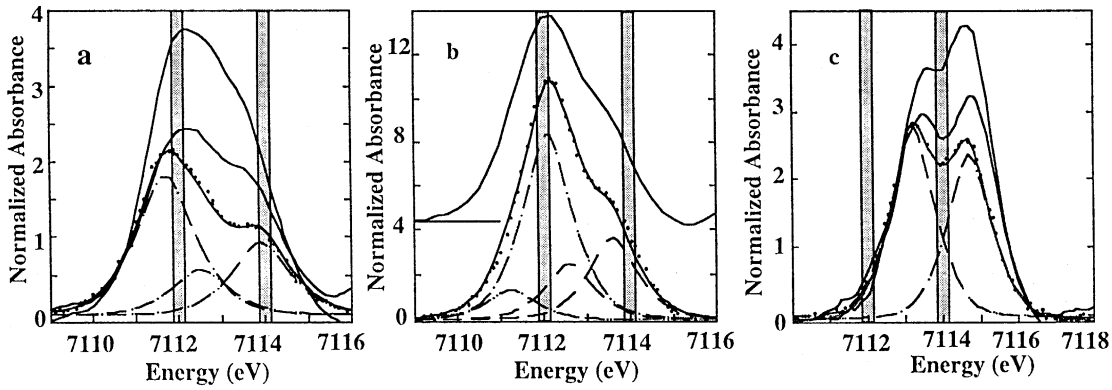

Fig. 3. Normalized pre-edge spectra extracted from the K-edge XANES spectra of Fe reference minerals. (a) From bottom to top: $^{6}Fe^{2+}$ in a slightly distorted octahedral site (siderite: dotted line, experimental spectrum; plain line: fit), and the three pseudo-Voigt components (dashed line) corresponding to the electronic transitions to 3d-like electronic levels; $^{6}Fe^{2+}$ in the distorted octahedral M1 and M2 sites of fayalite; $^{6}Fe^{2+}$ in the strongly distorted M2 site of hypersthene. (b) Bottom to top: $^{4}Fe^{2+}$ in a slightly distorted tetrahedral site (staurolite: dotted line, experimental spectrum; plain line: fit), and the four pseudo-Voigt components (dashed line) corresponding to the electronic transitions to 3d-like electronic levels; $^{4}Fe^{2+}$ in a regular tetrahedral site (spinel). (c) Bottom to top: $^{6}Fe^{3+}$ in a slightly distorted octahedral site (andradite: dotted line, experimental spectrum; plain line: fit), and the two pseudo-Voigt components (dashed line) corresponding to the electronic transitions to 3d-like electronic levels; $^{6}Fe^{3+}$ in the slightly distorted octahedral site of nontronite; $^{6}Fe^{3+}$ in the more distorted octahedral site of acmite. The shaded zones represent the position of the contribution of Fe^{2+} and Fe^{3+} at 7112 and 7114 eV, respectively.

(Fig. 3b), and correspond to the expected transitions (Fig. 2b). Their position and assignment are reported in Table 2. The similarity of the pre-edge spectrum in $FeAl_2O_4$ spinel, in which Fe^{2+} is located in a regular tetrahedral site, shows that the influence of site distortion is negligible in tetrahedral site (Fig. 3b). An important conclusion of this study is that the mean weighted position of the ^{4}F electronic transitions of the pre-edge features (centroid position) for staurolite and spinel is similar to that observed for Fe^{2+} in an octahedral site (7112 eV).

Table 2
Position and intensity of the pseudo-Voigt components and assignment of the corresponding final state in a $(Z+1)$ model

Minerals	Position (eV)[a]	Intensity[b]	Final state
Siderite	7095.7	1.8	$^{4}T_{1g}$ (^{4}F)
	7096.5	0.6	$^{4}T_{2g}$ (^{4}F)
	7097.9	0.9	$^{4}T_{1g}$ (^{4}P)
Staurolite	7095.1	1.3	$^{4}A_{2}$ (^{4}F)
	7096.1	8.3	$^{4}T_{2}$ (^{4}F)
	7096.6	2.4	$^{4}T_{1}$ (^{4}F)
	7097.6	3.5	$^{4}T_{1}$ (^{4}P)
Andradite	7097.2	2.7	$^{5}T_{2g}$ (^{5}D)
	7098.6	2.3	^{5}Eg (^{5}D)
FePO4	7098.0	13	^{5}E (^{5}D)
			$^{5}T_{2}$ (^{5}D)

[a] Error: ± 0.2 eV.
[b] Estimated uncertainty: ± 10%.

3.1.2. Fe^{3+} in octahedral and tetrahedral coordination

For Fe^{3+} in an octahedral site, two electronic transitions are expected from the 1s core level (Fig. 2c). These transitions are resolved, provided the instrumental resolution (1.5 eV: see above) is high enough. As an octahedral crystal field splitting is high enough ($\Delta o = 1.5$ eV) to give two contributions, which will appear well separated in the pre-edge spectrum, the small value of the tetrahedral crystal field, 0.67 eV ($4/9\ \Delta o$), will give an unsplit edge, due to the lack of spectral resolution.

Pre-edge spectroscopy of octahedral Fe^{3+} has been investigated in andradite, in which the Fe site is only weakly distorted (Q.E. = 1.0004). The pre-edge is made of two peaks of almost the same intensity; their position, relative intensity and transition assignment are given in Table 2. The mean weighted position of the ^{5}D electronic transitions of the pre-edge features (centroid position) (7114 eV) is moved by +2 eV, relative to that of Fe^{2+} pre-edge. The intensity of the highest component of the pre-edge, 2,7, is enhanced 1.3 time relative to that of Fe^{2+} in

regular octahedral coordination (Fig. 3c). Two pseudo-Voigt components, with a fixed FWHM value of 1.5 eV, fit the pre-edge, as expected from the above-mentioned considerations. Similar intensity values are found in pre-edge spectra of coordination compounds with octahedral Fe^{3+} (Westre et al., 1997). Site distortion, as in acmite (Q.E. = 1.0131) and nontronite, exerts a strong influence on the pre-edge shape and intensity (Fig. 3c). The intensity of the Fe^{3+} pre-edges in nontronite and acmite are enhanced by 1.1 and 1.5, respectively, as compared to andradite, and the relative intensity of the two components are inverse relative to andradite. These observations are in accordance with a stronger hybridization of the 3d and 4p levels in distorted sites (Galoisy et al., 1999).

Fe^{3+} in a tetrahedral site has been studied in Fe-berlinite (FePO4) (Combes et al., 1989; Manceau et al., 1990). Only one intense component is observed, giving this pre-edge a peculiar shape. This pre-edge has a pure pseudo-Voigt shape, keeping the fixed FWHM value of 1.5 eV. The strong enhancement of the intensity of the pre-edge, 13, is similar to that observed in the pre-edge spectra of coordination compounds with tetrahedral Fe^{3+} (Westre et al., 1997). Pre-edge maximum occurs at 7097.9 eV (Fig. 3c): as observed for Fe^{2+}, the position of the pre-edge of ferric iron in a tetrahedral site is identical to the centroid position of Fe^{3+} in an octahedral site (7114 eV). This centroid is moved by +1.5 eV relative to the centroid position of the pre-edge of Fe^{2+}.

3.2. Site distribution

As silicate glasses show the coexistence of various cation site geometries, it is necessary to see the influence of site distribution on pre-edge spectroscopy. Some problems may arise when the pre-edge results from the contribution of components with different normalized absorbancies. In the case of the coexistence of tetrahedral and octahedral sites, the former may give pre-edges more intense by a factor 3–4 than the latter. We have then fitted the pre-edge of YIG (Fig. 4), a garnet that contains 60% and 40% of $^{4}Fe^{3+}$ and $^{6}Fe^{3+}$. The centroid position of the experimental pre-edge spectrum is the same as for the other Fe^{3+} reference compounds investigated, a confirmation that pre-edge position is mostly independent of site geometry. The pre-edge intensity, 9, is intermediate between that of the pre-edge of $^{6}Fe^{3+}$ and $^{4}Fe^{3+}$. The pre-edge spectrum of YIG was fitted with a linear combination of the components used to fit the pre-edge spectra of Fe-berlinite ($^{4}Fe^{3+}$) and andradite ($^{6}Fe^{3+}$). As there is a priori no relation between the intensity of the pre-edge of $^{6}Fe^{3+}$ and $^{4}Fe^{3+}$, the sum of the two contributions is not constrained to be 100% and may be used to confirm the validity of the fitting procedure. The fit has been achieved with 64% and 26% of $^{4}Fe^{3+}$ and $^{6}Fe^{3+}$. A discrepancy of about 10% is, thus, found between the calculated and experimental contributions, probably due to an underestimated evaluation of the $^{6}Fe^{3+}$ contribution. As the site symmetry of $^{6}Fe^{3+}$ is the same in the two garnets investigated, there is no expected modification of the pre-edge intensity of $^{6}Fe^{3+}$. The observed deviation may then arise from the difficulty of extracting a pre-edge of low-intensity from the experimental XANES spectrum (uncertainty of ≈ 10%).

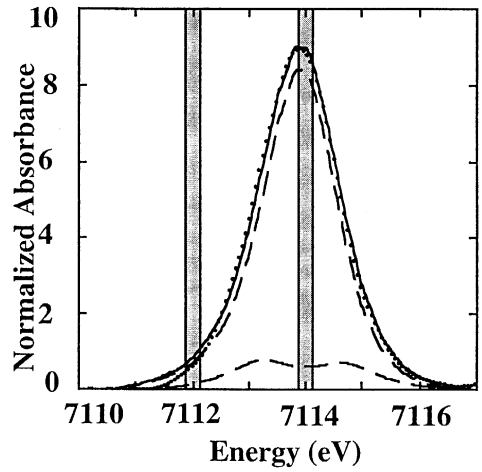

Fig. 4. Fe pre-edge extracted from the Fe^{3+}-K edge XANES spectrum of iron–yttrium garnet (dotted line). The fit obtained using pseudo-Voigt components of $^{6}Fe^{3+}$ and $^{4}Fe^{3+}$ (dotted lines) is represented as a full line. The shaded zones represent position of the contribution of Fe^{2+} and Fe^{3+} at 7112 and 7114 eV, respectively.

3.3. Pre-edge spectroscopy of synthetic glasses

In the synthetic augite glass, iron is only present as Fe^{2+}. The position of the pre-edge is in accor-

dance with the position of the above studied Fe^{2+} references (Table 3) and gives a confirmation of the absence of Fe^{3+} in the glass. Pre-edge intensity excludes the possibility of the presence of only sixfold-coordinated ferrous iron in this glass. It is intermediate between that of $^{6}Fe^{2+}$ in siderite and that of $^{4}Fe^{2+}$ in staurolite (Fig. 5). The local environment of ferrous iron in glasses is still debated, due to the apparent inconsistency of the various spectroscopic data available. Optical spectroscopy of various silicate glasses has been interpreted with Fe^{2+} in distorted octahedra (Fox et al., 1982; Keppler, 1992). Mössbauer and EXAFS spectroscopy suggested the presence of $^{4}Fe^{2+}$ or $^{5}Fe^{2+}$ in glasses (Calas and Petiau, 1983b; Waychunas et al., 1988; Jackson et al., 1990; Brown et al., 1995). More recently, Mössbauer spectroscopy and Fe-K edge EXAFS in a $CaFeSi_2O_6$ glass have shown the existence of a continuous site distribution from $^{4}Fe^{2+}$ to $^{5}Fe^{2+}$ (Rossano et al., 1999a,b). Regarding pre-edge spectroscopy, it has been shown that the intensity of the pre-edge varies inversely with the coordination number (i.e., I (octa) < I (fivefold-coordinated) < I (tetra)) and with a departure from a centrosymmetric environment (Roe et al., 1984; Randall et al., 1995). As for pre-edges of five-coordinated Fe^{2+} (Westre et al., 1997), the pre-edge of the augite glass is made of one apparent major band corresponding to the $1s\varnothing\ ^{4}B_2$ (^{4}F) transition, occurring at 7112 eV. The pre-edge intensity of the augite glass is, thus, in accordance with majority $^{5}Fe^{2+}$ and is not inconsistent with a site distribution including also $^{4}Fe^{2+}$.

Table 3
Apparent position and intensity of the pre-edge components in the glasses studied

Glass	Position (eV)[a]	Intensity[b]
Augite glass	7096.0	5.3
$Na_2Si_2O_5$:Fe	7098.0	10.8
Erta'Ale basalt	7096.2	4.0
	7097.7	2.5
Oxidized basalt	7096.1	3.5
	7097.7	4.7
Pantellerite (Boina)	7096.1	3.6
	7097.8	5.1

[a] Error: ± 0.2 eV.
[b] Estimated uncertainty: ± 10%.

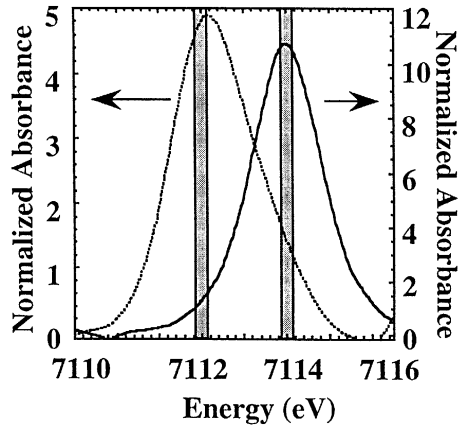

Fig. 5. Fe pre-edge extracted from the K-edge XANES spectrum of Fe in the synthetic augite glass (dotted line) and the $Na_2Si_2O_5$ glass (plain line). The position of the two pre-edges are in accordance with the expected position of the contribution of Fe^{2+} and Fe^{3+} at 7112 and 7114 eV, respectively. The differences in absorbance values arise from different coordination states of iron in these glasses.

In $Na_2Si_2O_5$/Fe glass, the pre-edge position (7114 eV) confirms the presence of Fe^{3+} as the main Fe oxidation state (Fig. 5). The width and intensity of the pre-edge are in agreement with the presence of only tetrahedral Fe^{3+} as evidenced in previous studies (Mysen, 1988). EXAFS data on the alkali silicate glasses (Calas and Petiau, 1983b; Henderson et al., 1995; Brown et al., 1995) are also consistent with $^{4}Fe^{3+}$. The presence of about 15% Fe^{2+} (Fox et al., 1982) explains a lower intensity than in the Fe-berlinite reference, as well as the slight asymmetry of the pre-edge. However, the possible presence of two distinct sites occupied by tetrahedral ferric iron, revealed by luminescence spectroscopy of sodium silicate glasses (Fox et al., 1982), cannot be confirmed by pre-edge spectroscopy.

3.4. Oxidation states of iron and site occupancy in volcanic glasses

3.4.1. Basaltic glass from Erta'Ale (Ethiopia)

The iron pre-edge spectrum of this volcanic glass is broader than in Fe^{2+} or Fe^{3+} references, due to the presence of both Fe^{2+} and Fe^{3+}. It consists of two distinct contributions: a major peak at 7112 eV

(apparent intensity of 4) and a shoulder at higher energy, 7114 eV (apparent intensity of 2.6) (Fig. 6a). These values correspond to the above-mentioned position for the Fe^{2+} and Fe^{3+} pre-edges with an apparent major contribution of Fe^{2+}. Previous spectra (Delaney et al., 1996, 1998), obtained under low spectral resolution, indicated an apparent shift of the pre-edge as a function of the Fe oxidation state. The instrumental resolution under the experimental conditions used in this study, about 1.5 eV, allows the resolution of the two contributions from Fe^{2+} and Fe^{3+} oxidation states, separated by 2 eV, which contribute to the total pre-edge in a bimodal distribution model.

The ferrous contribution in the iron pre-edge spectrum of the basaltic glass has been fitted using the augite glass reference spectrum. This shows that the surrounding of ferrous iron is similar in both glasses. Another indication is the relative intensity of this reference spectrum, 0.78, which is consistent, though slightly underestimated, with the redox estimate in this glass from wet chemical analysis (82% Fe^{2+}: Table 1). Earlier spectroscopic studies of the ferrous iron structural surrounding in basaltic glasses indicated the presence of mostly $^{6}Fe^{2+}$ (Bell et al., 1976; Nolet et al., 1979; Dyar and Burns, 1981). XANES data indicate lower coordination numbers, mainly $^{5}Fe^{2+}$, which would be consistent with a similar polymerization of the two glasses. Such low coordination numbers have been found for other transition elements in silicate glasses, such as nickel (Galoisy and Calas, 1993). These low-coordinated sites may be interpreted as resulting from the structure dynamics, in which the melt rheology implies important motion at the atomic scale as indicated by high-temperature studies of silicate glasses and melts (see, e.g., Stebbins, 1995). These motions favor low coordination sites, which may be preserved at the glass transition temperature (Tg).

On the high-energy side of the pre-edge, the presence of an unsplit feature at 7114 eV indicates an apparent major contribution of $^{4}Fe^{3+}$. This feature is well reproduced by the linear combination procedure, using 0.09 and 0.06 of $^{4}Fe^{3+}$ and $^{6}Fe^{3+}$, indicating 0.15 total Fe^{3+}. If only $^{4}Fe^{3+}$ is considered, the intensity of the corresponding component would be higher than the 2.6 intensity of the 7114 eV shoulder. Furthermore, as Fe^{2+} partly absorbs at 7114 eV, an even lower contribution must be considered. Thus, the contribution of low-absorbing species, such as $^{6}Fe^{3+}$, is needed to fit the high-energy side of the spectrum. As for YIG, the $^{6}Fe^{3+}$ contribution is probably underestimated, owing to the difficulty of extracting a pre-edge of low-intensity from the XANES spectrum. The presence of $^{6}Fe^{3+}$ is an important feature of the basaltic glass. By contrast to alkali silicate glasses in which ferric iron is mainly fourfold-coordinated, the Mössbauer isomer shift increases with the ionization potential (Mysen, 1988). This modification might indicate the presence of

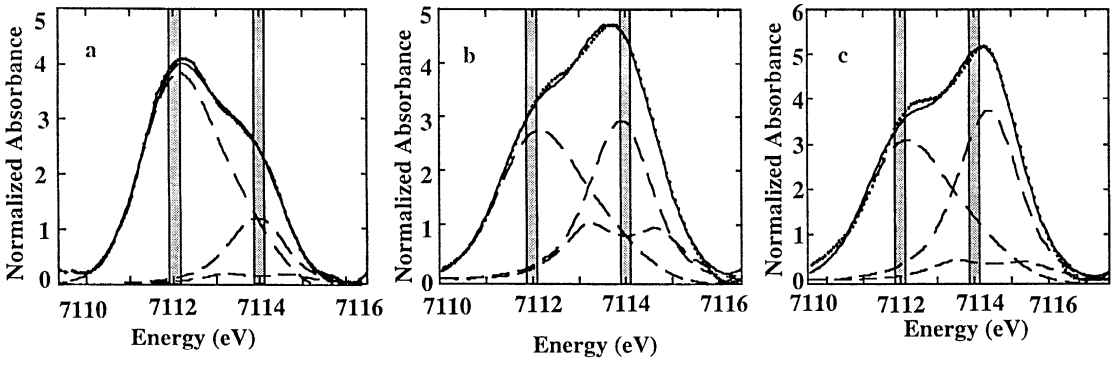

Fig. 6. Fe pre-edge extracted from the K-edge XANES spectra of volcanic glasses, Erta'Ale basaltic glass (a), oxidized basalt glass (b) and Boina pantelleritic glass (c). The dotted line indicates the experimental spectrum, the dashed lines represent an augite glass component (model for Fe^{2+} in glasses) and $^{4}Fe^{3+}$ and $^{6}Fe^{3+}$ components, and the plain line represents the fit. The shaded zones represent position of the contribution of Fe^{2+} and Fe^{3+} at 7112 and 7114 eV, respectively.

$^{6}Fe^{3+}$ in alkaline earth silicate glasses. In addition, $^{6}Fe^{3+}$ is also favored under reducing conditions, when Fe^{3+}/SFe is lower than 0.5 (Mysen, 1988). The high proportions of MgO and CaO and the low Fe^{3+}/SFe ratio in this glass might then explain the presence of significant amounts of $^{6}Fe^{3+}$. This result is consistent with existing Mössbauer spectra of basaltic glasses, which give Fe^{3+} Mössbauer isomer shifts intermediate between fourfold and sixfold-coordinated ferric iron, although the two contributions cannot be resolved by this method (Helgason et al., 1992). It is interesting that modal analyses indicate the presence of normative magnetite (2.91%: Barberi et al., 1973) as no magnetite crystals have been identified. The proportion of $^{4}Fe^{3+}$ and $^{6}Fe^{3+}$ in this basaltic glass well correlates with the site distribution in this phase.

3.4.2. Oxidized basaltic glass from the Holyoke Basalt Flow (USA)

This basaltic glass shows a pre-edge feature that shows the distinct contribution of the two Fe oxidation states, as observed for the previous basaltic glass. The different shape comes from different contribution of ferric and ferrous components. The position of the apparent maximum (Fig. 6b) and the shoulder observed at lower energy is consistent with the positions determined in pre-edge spectra of Fe^{2+} and Fe^{3+} references. In this glass, the major apparent contribution comes from Fe^{3+}, in which the fourfold coordination seems to dominate, as indicated by the absence of splitting. The sum of the various contributions to the whole fit is 1.13, with individual contributions from $^{6}Fe^{3+}$ and $^{4}Fe^{3+}$ and from Fe^{2+} of 0.35, 0.22 and 0.56, respectively.

This indicates an overestimate of the Fe-content of the glass, using these references, due to the presence of higher proportions of low-absorbing, high-coordinated ferric and ferrous iron. By contrast to that of ferrous iron, the estimate of ferric iron is consistent with wet chemical analysis (Bandyopadhyay et al., 1980), 57% and 52% Fe^{3+}, respectively.

The small visual deviation observed between the fit and the experimental spectrum around 7112 eV is probably related to a slight modification of the local environment around Fe^{2+} in the oxidized basaltic glass, in relation with the discrepancy observed between the contribution of Fe^{2+} estimated from pre-edge spectroscopy and that from chemical analysis. Fe^{2+} coordination may then be influenced by the oxidation process, with a higher proportion of sixfold-coordinated ferrous iron. The same observation holds for ferric iron, in which the apparent fourfold coordination corresponds indeed to a minority coordination state, as the majority of Fe^{3+} is sixfold-coordinated. Crystallization of magnetite at 700°C has been evidenced in this glass by Mössbauer and magnetic susceptibility measurements (Auric et al., 1982). The increase of $^{6}Fe^{3+}$ will favor the formation of this phase, as it is only normative in natural basaltic glasses (see above). In addition, the proportions of Fe^{3+} in fourfold and sixfold coordination, derived from high-resolution pre-edge spectra, may reflect some Fe ordering, making easier the nucleation of this phase at high temperature. Recent EXAFS measurements have shown the possibility of significant cation ordering in glasses that show a great ability to nucleate (Cormier et al., 1999). In that case, the medium range structure approximates that observed in the crystal, which will form from the glass/melt.

3.4.3. Pantelleritic glass from Boïna (Ethiopia)

The pre-edge spectrum has a shape similar to that of the oxidized basaltic glass, consistent with a major contribution of tetrahedral Fe^{3+} (Fig. 6c). Here too, the two contributions from Fe^{2+} and Fe^{3+} are resolved under the instrumental conditions chosen, a confirmation of the bimodal distribution of the ferrous and ferric contributions. The use of the augite glass as a reference for Fe^{2+} in this glass is not adapted, as the low-energy side of the spectrum is not correctly fitted. This may arise from the strong compositional difference between the augite reference glass and this more silicic volcanic glass (Barberi et al., 1974). By contrast, the Fe^{3+} contribution is correctly fitted with a mixture of $^{4}Fe^{3+}$ and $^{6}Fe^{3+}$. The sum of the various components of the fit shows an overall overestimate of 6%. The proportions of Fe^{2+} and Fe^{3+} derived from the fit are 0.63 and 0.43, respectively. These values are different from the values given by the wet chemical analysis, 50% Fe^{2+} and 50% Fe^{3+} (Barberi et al., 1974).

The CIPW norm of this rock is based on two normative phases for Fe^{2+} and Fe^{3+}, ferrosilite (8%) and acmite (10.2%), respectively (Barberi et al.,

1974). The acmite component might indicate the presence of $^{4}Fe^{3+}$ in the liquid, as the ferrosilite would be consistent with a simple Fe–Si chemical correlation. Pre-edge spectroscopy shows a more complex distribution of Fe coordination numbers, indicating various ways of chemical association between glass components. The deviation of the fit for the Fe^{2+} contribution is consistent with a stronger contribution of $^{4}Fe^{2+}$, which may be related to the more polymerized nature of the glass structure as compared to the augite glass. By contrast, Fe^{3+} is slightly underestimated, an indication of minor low-absorbing species with high coordination numbers, such as $^{6}Fe^{3+}$. The relative proportions of $^{6}Fe^{3+}$ and $^{4}Fe^{3+}$ are 0.15 and 0.28, respectively, indicating an increase of the proportion of $^{4}Fe^{3+}$, relative to the basaltic glasses investigated in this study. The presence of a minor $^{6}Fe^{3+}$ proportion is explained by the mildly reducing conditions, as a redox state of $Fe^{3+}/SFe = 0.5$ has been shown to favor the existence of high Fe^{3+} coordination states in alkali aluminosilicate glasses (Mysen and Virgo, 1989).

This pantelleritic glass correspond to the most differentiated, peralkaline term of the Boina volcanic series, in which oxidizing conditions are prevailing. Ferrous-ferric equilibria in simple glasses show that the ferric state is favored by an increasing glass basicity, i.e., at increasing alkali content (Thornber et al., 1980; Kilinc et al., 1983; Paul, 1990). The excess of alkalis in this peralkaline composition would favor the formation of $^{4}Fe^{3+}$, as they play a role of charge compensator. By contrast, the presence of alkaline earths in basaltic glasses favors $^{6}Fe^{3+}$, because of their low ability for charge compensating trivalent network formers (Navrotsky et al., 1985). The relative increase of $^{4}Fe^{3+}$ from basaltic to pantelleritic glasses may, in turn, give some structural support to the chemical dependence of redox equilibria. If the redox reaction is written in terms of simple ionic species, as:

$$4Fe^{2+}\,\text{glass} + O_2\,\text{glass} \rightleftarrows 4Fe^{3+}\,\text{glass} + 2O^{2-}\,\text{glass}, \quad (1)$$

then the redox equilibria show a chemical dependence, which is the opposite to what is observed, i.e., that ferric iron is favored as O^{2-} activity (i.e., melt basicity) decreases. The Holmquist expression accounts for the observed chemical dependence (Holmquist, 1966):

$$4FeO_{2^-} \rightleftarrows 4Fe^{2+} + 6O^{2-} + O_2. \quad (2)$$

High-resolution pre-edge spectra show that the relative proportion of $^{4}Fe^{3+}$, the FeO_{2^-} species in Eq. (2), is higher than $^{6}Fe^{3+}$ in peralkaline glasses relative to basaltic glasses. In a tetrahedral coordination, the Fe^{3+}–O bond is more covalent than in the higher coordination geometries. The modification of the average coordination of ferric iron in volcanic glasses results from the chemical dependence of the ferrous–ferric equilibria observed in magmatic systems.

4. Conclusion

Pre-edge spectroscopy appears to be a powerful method to determine redox and structural information around iron in synthetic and volcanic glasses. Pre-edge spectra can be reproduced with about 90% confidence using a linear combination between a Fe^{2+} augite glass and $^{4}Fe^{3+}$ and $^{6}Fe^{3+}$ references. The discrepancies observed between the redox values determined from high-resolution pre-edge spectroscopy and chemical analysis may arise from the pre-edge extraction from the main edge or from differences in the site geometry between the references used and the studied glass. Under high-resolution data acquisition, the pre-edges appear to result from a bimodal distribution between both oxidation states, although under low spectral resolution the pre-edge may only show an apparent shift as a function of the Fe^{3+}/Fe^{2+} ratio. This study shows that important errors can be made in the quantitative determination of oxidation states if site geometry is not taken into account. An important set of information may also be gained on the sites occupied by ferrous and ferric iron in volcanic glasses. The importance of ^{6}Fe in basaltic glasses and the prevalence of ^{4}Fe in silicic pantelleritic glasses are a result of the structural mechanisms, which drive the redox equilibria in silicate melts. High-resolution pre-edge spectroscopy is then a new tool to investigate the evolution of iron surrounding in volcanic glasses.

Acknowledgements

We thank Pr. Dr. Dingwell and two anonymous referees for their constructive comments. We thank the staff of LURE (Orsay) for their help in XANES measurements. This is IPGP contribution #.

References

Auric, P., Dang, N.V., Bandyopadhyay, A.K., Zarzycki, J., 1982. Superparamagnetic and ferrimagnetism of the small particle of magnetite in a silicate matrix. J. Non-Cryst. Solids 50, 97–106.

Bajt, S., Sutton, S.R., Delaney, J.S., 1994. X-ray microprobe analysis of iron oxidation in silicates and oxides using X-ray absorption near edge structure (XANES). Geochim. Cosmochim. Acta 58, 5209–5214.

Bandyopadhyay, A.K., Zarzycki, J., Auric, P., Chappert, J., 1980. Magnetic properties of a basalt glass and glass-ceramics. J. Non-Cryst. Solids 40, 353–368.

Barberi, F., Cheminée, J.L., Varet, J., 1973. Long-lived lava lakes of Erta Ale volcano. Rev. Geogr. Phys. Geol. Dyn. 15, 347–351.

Barberi, F., Santacroce, R., Varet, J., 1974. Silicic peralkaline volcanic rocks of the Afar depression (Ethiopia). Bull. Volcanol. 38, 1–24.

Bell, P.M., Mao, H.K., Weeks, R.A., 1976. Optical spectra and electron paramagnetic resonance of lunar and synthetic glasses: a study of the effects of controlled atmosphere, composition and temperature. Proc. Lunar Planet. Sci., 7th, 2543–2559.

Brown Jr., G.E., Calas, G., Waychunas, G.A., Petiau, J., 1988. X-ray absorption spectroscopy and its applications to mineralogy and geochemistry. In: Hawthorne, F. (Ed.), Spectroscopic Methods in Mineralogy and Geology. Rev. Mineral., vol. 18.

Brown, G.E., Farges, F., Calas, G., 1995. X-Ray Scattering and X-Ray Spectroscopy Studies of Silicate Melts. In: Stebbins, J.F., McMillan, P.F., Dingwell, D.B. (Eds.), Structure, Dynamics and Properties of Silicate Melts. Rev. Mineral., vol. 32, pp. 317–410.

Calas, G., Petiau, J., 1983a. Coordination of iron in oxide glasses through high resolution K-edge spectra: information from the pre-edge. Solid State Commun. 48, 625–629.

Calas, G., Petiau, J., 1983b. Structure of oxide glasses. Spectroscopic studies of local order and crystallochemistry. Geochemical implications. Bull. Mineral. 106, 33–55.

Combes, J.M., Manceau, A., Calas, G., Bottero, Y., 1989. Formation of ferric oxides from aqueous solutions: a polyhedral approach by X-ray absorption spectroscopy: I. Hydrolysis and formation of ferric gels. Geochim. Cosmochim. Acta 53, 583–594.

Cooney, T.F., Sharma, S.K., 1990. Structure of glasses in the systems Mg_2SiO_4–Fe_2SiO_4, Mn_2SiO_4–Fe_2SiO_4, Mg_2SiO_4–$CaMgSiO_4$, and Mn_2SiO_4–$CaMnSiO_4$. J. Non-Cryst. Solids 122, 10–32.

Cormier, L., Galoisy, L., Calas, G., 1999. Evidence of ordered domains in nickel-bearing alkali borate glasses. Europhys. Lett. 45, 572–578.

DeYoreo, J.J., Navrotsky, A., Dingwell, D.B., 1990. Energetics of the charge-coupled substitution Si–NaT in the glasses SiO_2–$NaTO_2$, T = (Al, Fe, Ga, B). J. Am. Ceram. Soc. 73, 2068–2072.

Delaney, J.S., Bajt, S., Sutton, S.R., Dyar, M.D., 1996. In situ microanalysis of Fe^{3+}/SFe ratios in amphibole by X-ray absorption near edge structure (XANES) spectroscopy. In: Dyar, M.D., McCammon, C.A., Shaeffer, M.W. (Eds.), Mineral Spectroscopy: A Tribute to Roger G. Burns. Geochem. Soc. Spec. Publ., vol. 5, pp. 165–171.

Delaney, J.S., Dyar, M.D., Sutton, S.R., Bajt, S., 1998. Redox ratios with relevant resolution: solving an old problem by using the synchrotron microXANES probe. Geology 26, 139–142.

Dingwell, D.B., 1989. Shear viscosities of ferrosilicate liquids. Am. Mineral. 74, 1038–1044.

Dingwell, D.B., Brealey, M., 1988. Melt densities in the CaO–FeO–Fe_2O_3–SiO_2 system and the compositional-dependence of the partial molar volume of ferric iron in silicate melts. Geochim. Cosmochim. Acta 52, 2815–2872.

Dingwell, D.B., Virgo, D., 1987. The effect of oxidation state on the viscosity of melts in the system Na_2O–FeO–Fe_2O_3–SiO_2. Geochim. Cosmochim. Acta 51, 195–205.

Dingwell, D.B., Virgo, D., 1988. Melts viscosities in the Na_2O–FeO–Fe_2O_3–SiO_2 system and factors controlling the relative viscosities of fully polymerized silicate melts. Geochim. Cosmochim. Acta 52, 395–403.

Dingwell, D.B., Brealey, M., Dickinson Jr., J.E., 1988. Melt densities in the Na_2O–FeO–Fe_2O_3–SiO_2 system and the partial molar volume of tetrahedrally-coordinated Ferric iron in silicate melts. Geochim. Cosmochim. Acta 52, 2467–2475.

Dräger, G., Frahm, R., Materlick, G., Brümmer, O., 1988. On the multipole character of the X-ray transitions in the pre-edge structure of Fe K absorption spectra. Phys. Status Solidi 146, 287–294.

Dyar, M.D., Burns, R.G., 1981. Coordination chemistry of iron in glasses contributing to remote-sensed spectra of the moon. Proc. Lunar Planet. Sci. Conf., 12th, 695–702.

Fox, K.E., Furukawa, T., White, W.B., 1982. Transition metal ions in silicate melts: Part 2. Iron in sodium silicate glasses. Phys. Chem. Glasses 23, 169–178.

Galoisy, L., Calas, G., 1993. Structural environment of nickel in silicate glass/melt systems: I. Spectroscopic determination of coordination states. Geochim. Cosmochim. Acta 57, 3613–3626.

Galoisy, L., Calas, G., Arrio, M.A., 1999. High resolution XANES spectra of iron in minerals and glasses: information from the pre-edge region. EOS Trans. 80, F1114.

Helgason, B., Steinthorsson, S., Morup, S., 1992. Rates of redox reactions in basaltic melts determined by Mössbauer spectroscopy. Hyperfine Interact. 70, 985–988.

Henderson, C.M.B., Cressey, G., Redfern, S.A.T., 1995. Geological applications of synchrotron radiation. Radiat. Phys. Chem. 45, 459–481.

Holmquist, S., 1966. Ionic formulation of redox equilibria in glass melts. J. Am. Ceram. Soc. 49, 228–229.

Jackson, W.E., Brown Jr, G.E., Waychunas, G.A., Mustre de leon, J., Conradson, S.D., Combes, J.M., 1990. In-situ high-temperature X-ray absorption study of ferrous iron in orthosilicate crystals and liquids. In: Hasnain, S.S. (Ed.), X-Ray Absorption Fine Structure. Ellis Horwood, Chichester, pp. 298–301.

Jackson, W.E., Brown Jr., G.E., Waychunas, G.A., Mustre de Leon, J., Conradson, S., Combes, J.-M., 1993. High-temperature XAS study of Fe_2SiO_4: evidence for reduced coordination of ferrous iron in the liquid. Science 262, 229–233.

Keppler, H., 1992. Crystal field spectra and geochemistry of transition metal ions in silicate melts and glasses. Am. Miner. 77, 62–75.

Kilinc, A., Carmichael, I.S.E., Rivers, M.L., Sack, R.O., 1983. Ferric–ferrous ratio of natural silicate liquids equilibrated in air. Contrib. Miner. Petrol. 83, 136–141.

Kostov, R.I., Yanev, Y., 1996. EPR data on volcanic siliceous glasses ferom the eastern Rhodopes (Bulgaria) and the Lipari Island (Italy). Appl. Magn. Reson. 10, 431–438.

Manceau, A., Gates, W.P., 1997. Surface structural model for ferrihydrite. Clays Clay Miner. 45, 448–460.

Manceau, A., Combes, J.M., Calas, G., 1990. New data and a revised structural model for ferrihydrite: a comment. Clays Clay Miner. 38, 331–334.

Mysen, B.O., 1988. Structure and Properties of Silicate Melts. Elsevier, 354 pp.

Mysen, B.O., Virgo, D., 1989. Redox equilibria, structure and properties of Fe-bearing aluminosilicate melts: relationships among temperature, composition and oxygen fugacity in the system $Na_2O–Al_2O_3–SiO_2–Fe–O$. Am. Miner. 74, 58–76.

Navrotsky, A., Geisinger, K.L., McMillan, P., Gibbs, G.V., 1985. The tetrahedral framework in glasses and melts — inferences from molecular orbital calculations and implications for structure, thermodynamics and physical properties. Phys. Chem. Miner. 11, 284–298.

Nolet, D.A., Burns, R.G., Flamm, S.L., Besancon, J.R., 1979. Spectra of Ti–Fe silicate glasses: implications to remote-sensing of planetary surfaces. Proc. Lunar Planet. Sci. Conf., 10th, 1775–1786.

Paul, A., 1990. Chemistry of Glasses. Chapman & Hall, London, New York, 367 pp.

Randall, C.R., Shu, L., Chiou, Y.M., Hagen, K.S., Ito, M., Kitajima, N., Lachicotte, R.J., Zang, Y., Lawrence Jr., Q., 1995. X-ray absorption pre-edge studies of high spin iron (II) complexes. Inorg. Chem. 34, 1036–1039.

Regnard, J.R., Chavez-Rivas, F., Chappert, J., 1981. Study of the oxidation states and magnetic properties of iron in volcanic glasses: Lipari and Teotohuacan obsidians. Bull. Mineral. 104, 204–210.

Robinson, K., Gibbs, G.V., Ribbe, P.H., 1971. Quadratic elongation: a quantitative measure of distortion in coordination polyhedra. Science 172, 567–570.

Roe, A.L., Schneider, D.J., Mayer, R.J., Pyrz, J.W., Widom, J., Que Jr., L., 1984. X-ray absorption spectroscopy of iron-tyrosinate proteins. J. Am. Chem. Soc. 106, 1676–1681.

Rossano, S., Balan, E., Morin, G., Bauer, J.-P., Calas, G., Brouder, C., 1999a. ^{57}Fe Mössbauer spectroscopy of tektites. Phys. Chem. Miner. 26, 530–538.

Rossano, S., Ramos, A., Delaye, J.M., Filipponi, A., Creux, S., Brouder, Ch., Calas, G., 1999b. Iron surrounding in $CaO–FeO_2–SiO_2$ glass: EXAFS and molecular dynamics simulation. J. Synchrotron Radiat. 6, 247–248.

Scott, R.A., Hahn, J.E., Doniach, J., Freeman, H.C., Hodgson, K.O., 1982. Polarized X-ray absorption spectra of oriented plastocyanin single crystals. Investigation of methionine–copper coordination. J. Am. Chem. Soc. 104, 5364.

Shulman, R.G., Yafet, Y., Eienberger, P., Blumberg, W.E., 1976. Observations and interpretation of X-ray absorption edges in iron compounds and proteins. Proc. Natl. Acad. Sci. 73, 1384–1388.

Stebbins, J.F., 1995. Dynamics and structure of silicate and oxide melts: nuclear magnetic resonance studies. In: Stebbins, J.F., McMillan, P.F., Dingwell, D.B. (Eds.), Structure, Dynamics and Properties of Silicate Melts. Rev. Mineral. vol. 32, pp. 191–246.

Thornber, C.R., Roeder, P.L., Foster, J.R., 1980. The effect of composition on the ferric–ferrous ratio in basaltic liquids at atmospheric pressure. Geochim. Cosmochim. Acta 44, 525–532.

Waychunas, G.A., Apted, M.J., Brown Jr., G.E., 1983. X-ray K-edge absorption spectra of Fe minerals and model compounds: near edge structure. Phys. Chem. Miner. 10, 1–9.

Waychunas, G.A., Brown Jr., G.E., Ponader, C.W., Jackson, W.E., 1988. Evidence from X-ray absorption for network-forming Fe^{2+} in molten alkali silicates. Nature (London) 350, 251–253.

Westre, T.A., Kennepohl, P., DeWitt, J.G., Hedman, B., Hodgson, K.O., Solomon, E.I., 1997. A multiplet analysis of Fe K-edge 1s∅3d pre-edge features of iron complexes. J. Am. Chem. Soc. 119, 6297–6314.

Wong, J., Lytle, F.W., Messmer, R.P., Maylotte, D.H., 1984. K-edge absorption spectra of selected vanadium compounds. Phys. Rev. [Sect.] B 30, 5596–5610.